Hindawi
Advances in Civil Engineering
Volume 2022, Article ID 2976271, 19 pages
https://doi.org/10.1155/2022/2976271

Research Article

Research on the Vibration Isolation Characteristics of Floor Vibration Isolation Slab System under Train Operation

Jinbao Yao, Han Wu, and Shaoyin Tao

School of Civil Engineering, Beijing Jiaotong University, Beijing 100044, China

Correspondence should be addressed to Jinbao Yao; jbyao@bjtu.edu.cn

Received 10 June 2022; Revised 20 July 2022; Accepted 12 August 2022; Published 12 September 2022

Academic Editor: Quanmin Liu

This study takes the vibration isolation measures of building floor vibrations induced by trains as the starting point and carries out both theoretical derivation and numerical simulation. A four-degree-of-freedom (DOF) multi-dimensional vibration isolation platform (VIP) dynamics model is established based on the theoretical research of single-level, single-degree-of-freedom vibration isolation systems. Under multi-point excitation, the model can deduce the horizontal and vertical vibration responses of the VIP system. A comprehensive analysis of the vibration isolation performance of the VIP system on the floor and how the variation of the parameters influences the performance of the vibration isolation systems are presented. Several variables, such as the thickness, stiffness, damping ratio, and the number of isolators of the VIP system, are theoretically found to have a significant impact on the vibration isolation effect of the floor VIP system. Empirical results show that the VIP system significantly affects the vibration isolation of the building floor induced by a train and has the best vibration isolation effect on the acceleration response and the worst vibration isolation effect on the displacement response.

1. Introduction

With the rapid development of China's transportation industry, the environmental vibration problems caused by train operations have become increasingly prominent. At the same time, as people's demand for quality of life continues to increase, higher demands are being placed on the control of environmental vibrations, and research on the environmental problems caused by train vibrations and vibration isolation measures have attracted considerable attention from scholars [1]; Forrest and hunt, 2006; [2–4]. At present, there are three main types of control measures for the impact of train vibrations on the surrounding environment: control of the vibration source, control of the propagation path, and control of the vibrated body. Among them, the installation of secondary vibration isolation platforms (VIP) inside buildings has become a popular research topic for many scholars.

Ungar et al. [5] first classified the main sources of vibrations associated with high-technology equipment into three categories: external sources (microseismic and seismic, nearby road or rail traffic, and construction activities), internal sources (personnel walking, service activities, and production work), and service machinery (all electromechanical equipment in buildings). Hwang et al. [6] evaluated the applicability of seismic protection systems in high-technology industrial structures in Earthquake-prone areas and compared the protective performances of structures against microseismic activity before and after the implementation of microseismic protection systems. They proposed that there is nonnegligible coupling between the plant structure and its internal vibration isolation plate system in the horizontal direction, and by establishing a single/double hybrid platform coupled with the building structure, a combination of experiments and numerical simulations was used to control the microvibrations of high-technology equipment [7–10]. Yang et al. [11] conducted a numerical analysis of a large building near a metro network, proposed a two-stage time-frequency prediction method for predicting the superstructure's vibration response, and evaluated building vibration using two related criteria. Ibrahim [12] introduced the basic concepts and characteristics of

nonlinear vibration isolators and the inherent nonlinear phenomena. Specific types of nonlinear vibration isolators are then discussed, including ultralow frequency isolators. Lazar et al. [13] proposed to inert a novel passive vibration control system in a multi-story building and compared an inertial agent-based system with a tuned mass damper (TMD) system. It demonstrates that the potential performance of vibration control will be improved through the use of an inertial agent rather than a TMD.

Domenico et al. [14] proposed an enhanced base seismic isolation system, a TMD inertia device (TMDI). They found that when the inertia device is installed in series with a spring and damper element, a lower-mass and more efficient alternative to conventional TMDs is obtained, finding the optimum parameters of the TMDI based on a probabilistic framework by using the time history analysis of isolated multi-story buildings under several seismic excitations to assess the effectiveness of the optimal TMDI parameters. Yun et al. [15] proposed the novel design of a dual redundant parallel robot. It enabled the positioning of high or rough precision and realized 6-DOF active vibration isolation and excitation of payloads on a moving platform; Gardonio et al. [16] proposed a multi-degree-of-freedom system to evaluate the dynamics of active isolation systems for structural vibrations; Kumar and Whittaker [17] proposed cross-platform implementation, verification, and validation of advanced mathematical models for elastic vibration isolation bearings; Farsangi et al. [18] proposed a shaking isolation system called the "telescopic column" (TC) and investigated an elastic low-damage base isolation system under combined vertical and horizontal excitations; and Yang and Agrawal [19] conducted an extensive numerical study on whether hybrid control isolation systems can be applied to microvibrations.

The structure of this study is organized as follows: Section 2 is based on the theory of single-layer VIP systems, establishing a four-degree-of-freedom multi-dimensional VIP system model. In addition, Sections 3,4, and 5 show that the vibration isolation effect of floor VIP systems under external excitation is analyzed more comprehensively, and the influence of VIP structural parameters on the vibration isolation effect is also studied. The conclusions are presented in Section 6.

2. Theoretical Research on Vibration Isolation in VIP Systems

2.1. Theoretical Analysis of Single-Degree-of-Freedom Vibration Isolation. The performance evaluation criterion of a single-degree-of-freedom vibration isolation system is the transmission efficiency of the vibration isolation system T_r. The value of T_r directly reflects the attenuation level of vibrations through vibration isolation systems and can effectively measure the vibration isolation effect of vibration isolation systems. The formula for the vibration isolation efficiency of a single-layer passive vibration isolation system is

$$T_r = \sqrt{\frac{1 + \left[2\xi\left(\omega/\omega_n\right)\right]^2}{\left[1 - \left(\omega/\omega_n\right)^2\right]^2 + \left[2\xi\left(\omega/\omega_n\right)\right]^2}}. \quad (1)$$

In (1), the smaller the value of T_r for vibration isolation efficiency is, the better the vibration isolation effect; ω is the external interference circle frequency (rad/s), ω_n is the self-circular frequency of the vibration isolation structure (rad/s); and ξ is the vibration isolator damping ratio.

2.2. Dynamic Analysis of a Single-Layer Multi-Dimensional VIP System under Multi-Point Excitation. With the increase in the number of vibration isolators on the VIP arrangement, the number of points of external excitation that vibration isolators are subjected to increases, and the vibration response of the VIP system changes from a single degree to multiple degrees of freedom.

2.2.1. Multidimensional Vibration Isolator System Dynamics Model. A vibration isolation system has three axes of translational motion and rotation along these three directions. The vibration isolation system's horizontal and vertical vibration response is the main form of vibration that triggers the secondary structure. In this study, we only consider the coupled motion of the four degrees of freedom of the vibration isolation system, including the translational degrees of freedom in the direction of the three axes (X, Y, and Z) and the rotational degrees of freedom around the Y-axis.

Figures 1 and 2 show a simplified multi-dimensional vibration isolation plate system model, which, from top to bottom, shows the vibration isolation plate, spring isolator, and foundation base.

Some parameters of the vibration isolation plate system and the vibration isolator arrangement are set as follows: the length of the VIP is $2l$, the width of the platform is d, the thickness of the platform is H, the density is ρ; the bottom of the VIP is uniformly arranged with N vibration isolators. The horizontal Y direction of the platform is uniformly arranged with N spring vibration isolators, and the height of the vibration isolator arrangement is consistent with the center of gravity of the VIP. The horizontal X direction of the platform is uniformly arranged with n spring vibration isolators, assuming that the height of the vibration isolator arrangement is consistent with the center of gravity of the vibration isolation plate. The vertical height difference between the vibration isolator and the center of gravity of the VIP is h ($h \geq 0$). The stiffness and damping of the isolators arranged along the three translational directions are set as k_1, k_2, and k_3 and c_1, c_2 and c_3, respectively, and the disturbance excitations F_x, F_y, and F_z in the X, Y, and Z directions are shown in (2) according to Figure 1:

$$\begin{cases} F_x = p_m \sin\left(\omega_x t + \theta_m\right) \\ F_y = p_j \sin\left(\omega_y t + \gamma_j\right) \quad (i, j, m = 1 \ldots n). \\ F_z = p_i \sin\left(\omega_z t + \vartheta_i\right) \end{cases} \quad (2)$$

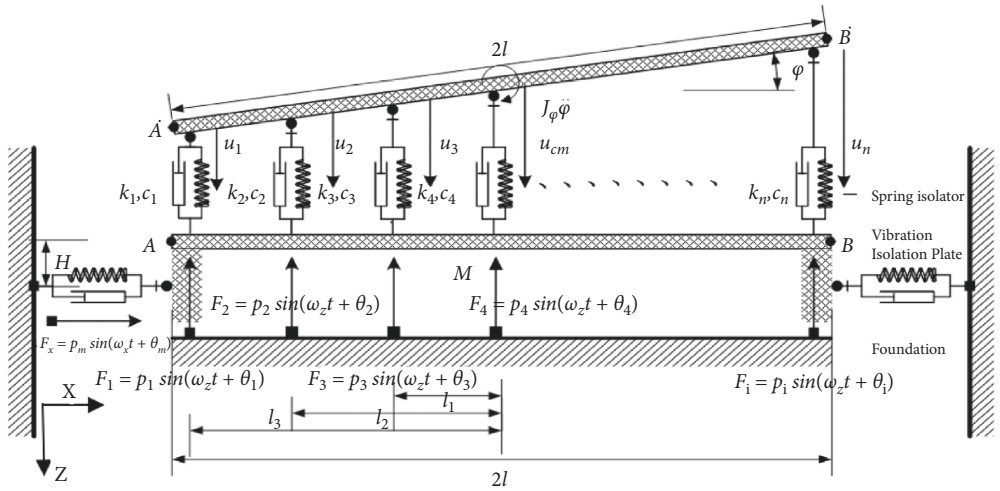

Figure 1: Multi-dimensional vibration isolation system (Front view).

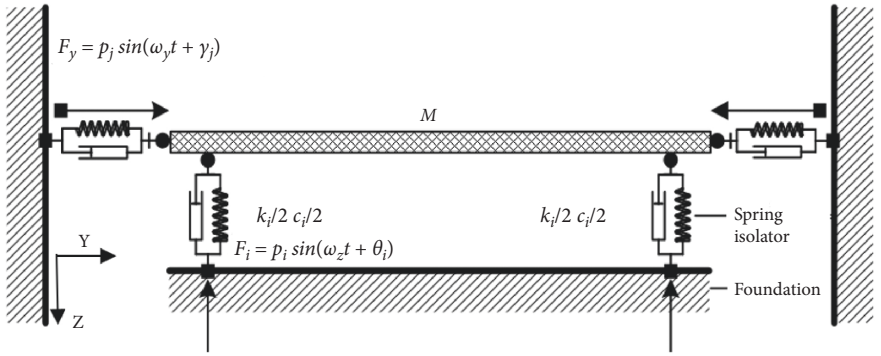

Figure 2: Multi-dimensional vibration isolation system (Side view).

When the stiffness and damping of the vibration isolators arranged under the vibration isolators are the same, $k_i = k_1$, and $c_i = c_1 (i = 1 \ldots n)$, the vertical degrees of freedom of the vibration isolators and the rotational degrees of freedom around the Y-axis are independent, are uncoupled and can be solved as single-degree-of-freedom systems, respectively.

u_{cm} and θ represent the generalized coordinates of the system; F_1 and F_2 represent the external disturbance forces; M represents the mass of the vibration isolator system; I_{c} represents the rotational inertia of the vibration isolator system; u_1 and u_n represent the vibration responses of the two ends of the vibration isolator system, where $u_1 = u_{\mathrm{cm}} - l_\theta$ and $u_{\mathrm{n}} = u_{\mathrm{cm}} + l_\theta$; θ indicates the rotational response of the vibration isolator.

2.2.2. Development of Differential Equations for the Vibration of a Multi-Dimensional Vibration Isolator System. For a complete constrained system of masses, the spatial position u_i of any mass m_i can be expressed as a function of its generalized coordinates $q_i (i = 1 \ldots n)$ and time, and for generalized coordinates $q_j = X, Y, Z, \varphi$; the corresponding generalized forces can be expressed by

$$\begin{cases} Q_x = \sum_{m=1}^{n} p_m \sin(\omega_x t + \theta_m), \\ Q_y = \sum_{j=1}^{n} p_j \sin(\omega_y t + \gamma_j), \\ Q_z = \sum_{i=1}^{n} p_i \sin(\omega_z t + \vartheta_i), \\ Q_\varphi = \sum_{i=1}^{n} p_i \sin(\omega_z t + \vartheta_i) l_i \zeta_i, \end{cases} \tag{3}$$

where Q_{y}, Q_{x}, Q_{z}, and Q_j represent the generalized forces corresponding to the four degrees of freedom of the isolation system; p_{m}, p_{j}, and p_{i} represent the amplitudes of the three directions of the external excitation in the isolation system; ω_{x}, ω_{y}, and ω_{z} represent the circular frequencies (rad/s) of the three directions of the external excitation in the isolation system; and θ_m, γ_j, and ϑ_i represent the phase angles of the three directions of the external excitation of the isolation system, ζ_i indicates the position coefficient of the spring isolator, value of ζ_i at the left and right sides of the center point of the plate is ± 1 respectively; l_i indicates the horizontal distance from the vibration isolator arranged at the

bottom of the vibration isolation plate to the center point of the plate.

The rotational inertia of the system along the direction is $I_y = \int (l^2 + h^2)dm$, as the thickness of the isolation plate, is much less than the length of the plate $2l$, so we can ignore the effect of the thickness of the isolation platform. The rotational inertia is expressed as $J_\varphi = 1/3Ml^2$. Bringing the energy formula derived in the previous summary into the Lagrange dynamics equations and replacing each degree of freedom of the VIP with the generalized coordinate q_j, the differential equations used for the dynamics of different degrees of freedom of the multi-dimensional vibration isolation system can be obtained, as shown in Equations (4)–(7).

(1) Vertical motion at the center of a multi-dimensional vibration isolator ($q_j = Z$) is represented as follows:

$$M\ddot{Z} + \sum_{i=1}^{n} k_i^3 Z + \sum_{i=1}^{n} c_i^3 \dot{Z} = \sum_{i=1}^{n} p_i \sin(\omega_z t + \vartheta_i). \tag{4}$$

(2) Rotation of multi-dimensional vibration isolators plate($q_j = \varphi$) is represented as follows:

$$J_\varphi \ddot{\varphi} + \sum_{i=1}^{n} k_i^1 \left(h^2 \varphi + hX\right) + \sum_{i=1}^{n} k_i^3 l_i^2 \varphi + \sum_{i=1}^{n} c_i^1 \left(h^2 \dot{\varphi} + h\dot{X}\right) + \sum_{i=1}^{n} c_i^3 l_i^2 \dot{\varphi} = \sum_{i=1}^{n} p_i \sin(\omega_z t + \vartheta_i) l_i \zeta_i. \tag{5}$$

(3) Horizontal movement of multi-dimensional vibration isolator plate($q_j = X$) is represented as follows:

$$M\ddot{X} + \sum_{i=1}^{n} k_i^1 (X + h\varphi) + \sum_{i=1}^{n} c_i^1 (\dot{X} + h\dot{\varphi}) = \sum_{m=1}^{n} p_m \sin(\omega_x t + \theta_m). \tag{6}$$

(4) Horizontal movement of multi-dimensional vibration isolator plate($q_j = Y$)is represented as follows:

$$M\ddot{Y} + \sum_{i=1}^{n} k_i^2 Y + \sum_{i=1}^{n} c_i^2 \dot{Y} = \sum_{j=1}^{n} p_j \sin\left(\omega_y t + \gamma_j\right). \tag{7}$$

$k_i^1, k_i^2, k_i^3$are the stiffness of the isolators in X, Y and Z directions respectively; c_i^1, c_i^2, c_i^3 are the damping of the isolators in X, Y and Z directions respectively.

2.3. Vibration Response of a Multi-Dimensional Vibration Isolator System under Multi-Point Excitation

2.3.1. Z-Directional Response of a Multi-Dimensional Vibration Isolator System under Multi-Point Excitation. Suppose that the external simple harmonic excitation $F_Z = p_i \sin(\omega_z t + \vartheta_i)$ is applied to the vibration isolator system by the arrangement of the vertical vibration isolator, thus causing the vertical vibration of the vibration isolator system. We take the central pickup point of the vibration isolator system as the research object, and then, the differential equation of the vertical response of the multi-dimensional vibration isolation system can be expressed by (4).

In equation (4), $k_i^3 = k_3$ represents the vertical vibration isolator spring stiffness, and $c_i^3 = c_3$ represents the vertical vibration isolator damping. The center point of the vertical displacement of the vibration isolator in the formula without the rotation angle φ and $\dot{\varphi}$item can be seen due to the influence of the vibration isolator, which is symmetrically arranged relative to the center point of the vibration isolator to the left and right; the position function ζ_i to the left and right sides show the opposite sign, so the parts of the formula containing φ and $\dot{\varphi}$ counteract each other. (4) can be expressed as follows:

$$M\ddot{Z} + nc_3\dot{Z} + nk_3 Z = \sum_{i=1}^{n} p_i \sin(\omega_z t + \vartheta_i). \tag{8}$$

The solution to the differential equation can be expressed as follows:

$$Z = u_i \sin(\omega_z t + \vartheta_i - \phi_i). \tag{9}$$

In the above formula, the following terms are utilized:

$$\begin{cases} u_i = u_{st} \dfrac{1}{\left[1 - (\omega_z/\omega_n)^2\right]^2 + \left[2\xi(\omega_z/\omega_n)\right]^2} \\ \phi_i = \arctan \dfrac{2\xi(\omega_z/\omega_n)}{1 - (\omega_z/\omega_n)^2} \end{cases}. \tag{10}$$

Considering the superposition ability of solutions to differential equations, the final solution to Equation (10) is therefore given as follows:

$$Z = \sum_{i=1}^{n} u_{st} \frac{1}{\left[1 - (\omega_z/\omega_n)^2\right]^2 + \left[2\xi(\omega_z/\omega_n)\right]^2} \sin(\omega_z t + \vartheta_i - \phi_i), \tag{11}$$

whereω_z represents the external disturbance circular frequency; $\omega_n$represents the vibration isolation structure's own circular frequency; ξ is the vibration isolator damping ratio; ϑ_i represents the initial phase angle of the external disturbance force; and $\vartheta_i - \phi_i$ represents the phase angle, reflecting the relationship between the system vibration displacement and the phase of the simple harmonic load.

2.3.2. Y-Directional Response of a Multi-Dimensional Vibration Isolator System with Multi-Point Excitation. According to (10), the horizontal Y-directional vibration response of this multi-dimensional vibration isolator system can also be reduced to the problem of a single-degree-of-freedom mass-spring system, similar to the z-directional response of vertical vibrations at the pickup point in the center of the vibration isolator, and can be solved in a similar manner and with similar results.

2.3.3. X-Direction and Y-Axis Rotation Response of a Multi-Dimensional Vibration Isolator System under Multi-Point Excitation. The horizontal X-directional degrees of freedom of the multi-dimensional vibration isolation system and the degrees of freedom of rotation around the *Y*-axis φ are coupled with each other, so the vibrations of the two degrees of freedom of the VIP are discussed together, and its dynamical differential equation matrix form can be introduced by (8) and (9) as follows:

$$\begin{bmatrix} M & \\ & J_\varphi \end{bmatrix}\begin{bmatrix} \ddot{X} \\ \ddot{\varphi} \end{bmatrix} + \sum_{i=1}^{n}\begin{bmatrix} c_i^1 & hc_i^1 \\ hc_i^1 & h^2c_i^1 + l_i^2c_i^3 \end{bmatrix}\begin{bmatrix} \dot{X} \\ \dot{\varphi} \end{bmatrix} + \sum_{i=1}^{n}\begin{bmatrix} k_i^1 & hk_i^1 \\ hk_i^1 & h^2k_i^1 + l_i^2k_i^3 \end{bmatrix}\begin{bmatrix} X \\ \varphi \end{bmatrix} = \begin{bmatrix} \sum_{m=1}^{n} p_m \sin(\omega_x t + \theta_m) \\ \sum_{i=1}^{n} p_i \sin(\omega_z t + \vartheta_i) l_i \zeta_i \end{bmatrix}, \tag{12}$$

where $k_i^1 = k_1$ is the horizontal vibration isolator spring stiffness and $c_i^1 = c_1$ is the horizontal vibration isolator damping.

It follows from the principle of the superposition of solutions to differential equations that the special solution to this equation consists of two parts, and we set the special solution to this equation as follows:

$$\begin{cases} X = H_{11}(\omega_x)F_1 + H_{12}(\omega_z)F_2, \\ \varphi = H_{21}(\omega_x)F_1 + H_{22}(\omega_z)F_2, \\ F_1 = \sum_{m=1}^{n} p_m \sin(\omega_x t + \theta_m), \\ F_2 = \sum_{i=1}^{n} p_i \sin(\omega_z t + \vartheta_i) l_i \zeta_i. \end{cases} \tag{13}$$

In this form, assume that the unique solution to the first part is as follows:

$$\begin{cases} X_{11} = H_{11}(\omega_x) e^{j(\omega_x t + \theta_m - \alpha)}, \\ \varphi_{21} = H_{21}(\omega_x) e^{j(\omega_x t + \theta_m - \alpha)}, \end{cases} \tag{14}$$

where ω_x is the circular frequency (rad/s) and θ_m-α is the initial phase angle; $j^2 = -1$.

By bringing in (15), we obtain the following:

$$\begin{bmatrix} nk_1 - M\omega_x^2 + in\omega_x c_1 & nh(k_1 + j\omega_x c_1) \\ nh(k_1 + j\omega_x c_1) & n\left(h^2k_1 + l^2k_3\right) - J_\varphi\omega_x^2 + jn\omega_x\left(h^2c_1 + l^2c_3\right) \end{bmatrix}\begin{bmatrix} H_{11}(\omega_x)e^{-j\alpha} \\ H_{21}(\omega_x)e^{-j\alpha} \end{bmatrix} = \begin{bmatrix} 1 \\ 0 \end{bmatrix}. \tag{15}$$

Equation (15) is expressed in the following form:

$$[Z]\begin{bmatrix} H_{11}(\omega_x)e^{-j\alpha} \\ H_{21}(\omega_x)e^{-j\alpha} \end{bmatrix} = \begin{bmatrix} 1 \\ 0 \end{bmatrix}. \tag{16}$$

Then, we obtain the following:

$$\begin{bmatrix} H_{11}(\omega_x)e^{-j\alpha} \\ H_{21}(\omega_x)e^{-j\alpha} \end{bmatrix} = [Z]^{-1}\begin{bmatrix} 1 \\ 0 \end{bmatrix} = \frac{1}{|Z|}\begin{bmatrix} n\left(h^2k_1 + k_3l^2\right) - J_\varphi\omega_x^2 + jn\omega_x\left(c_1h^2 + c_3l^2\right) \\ -nh(k_1 + j\omega_x c_1) \end{bmatrix}. \tag{17}$$

The final result is as follows:

$$\begin{cases} H_{11}(\lambda)e^{-j\alpha} = \dfrac{h^2 + l^2\lambda_2^2 - \mu\lambda_1^2 + j\lambda_1\left(2\xi_1h^2 + 2\xi_2l^2\lambda_2\right)}{\Delta\lambda nk_1}, \\ H_{21}(\lambda)e^{-j\alpha} = \dfrac{\left[h\lambda_1^2 + 2j\lambda_1\xi_1\right]}{\Delta\lambda nk_1}, \end{cases} \tag{18}$$

where

$$\lambda = \mu\lambda_1^4 - \lambda_1^2\left(l^2\lambda_2^2 + \mu\lambda_2^2 + 4\xi_1\xi_2\lambda_2^2l^2 + h^2\right) + l^2\lambda_2^2 - 2j\left(-\xi_2\lambda_1\lambda_2l^2 - \xi_1\lambda_1^2\lambda_2l^2 + \mu\xi_1\lambda_1^3 + \xi_1\lambda_1^3h^2 + \xi_2\lambda_1^3\lambda_2l^2\right). \tag{19}$$

The following parameters are introduced:

$$\mu = \frac{J_\varphi}{M}; \lambda_1 = \frac{\omega_x}{\omega_1}; \lambda_2 = \frac{\omega_3}{\omega_1}$$

$$\omega_1^2 = \frac{nk_1}{M}; \omega_3^2 = \frac{nk_3}{M}; \xi_1 = \frac{nc_1}{2M\omega_1} \quad . \tag{20}$$

$$\xi_2 = \frac{nc_3}{2M\omega_3}; \delta_1 = \frac{P_k}{nk_1}; \delta_2 = \frac{P_k}{nk_1}l_i\zeta_i$$

From Equation (21), $h_{11}(\lambda_x)e^{-j\alpha}$ represents the characteristics of a system with an input of force, and $h_{21}(\lambda_x)e^{-j\alpha}$ represents the characteristics of a system that outputs displacement; thus, its magnitude is $1/K$. According to the rules of complex arithmetic calculations,

$$\left|H_{21}(\lambda)\right| = \sqrt{\frac{\left(h\lambda_1^2\right)^2 + \left[(2j\lambda_1\xi_1)\right]^2}{\left[\mu\lambda_1^4 - \lambda_1^2\left(l^2\lambda_2^2 + \mu\lambda_2^2 + 4\xi_1\xi_2\lambda_2^2l^2 + h^2\right) + l^2\lambda_2^2\right]^2 + \left[\lambda_1^3(2)\mu\xi_1 + 2\xi_1h^2 + 2\xi_2\lambda_2l^2\right) - \lambda_1(2)\xi_2\lambda_2l^2 + 2\xi_1\lambda_1\lambda_2l^2)\right]^2}}. \tag{21}$$

Equation (19) is rewritten as follows:

$$H_{11}(\lambda_x) = \left|H_{11}(\lambda_x)\right|e^{j\phi_{11}(\lambda)} = \left(\frac{D_{11}^2 + E_{11}^2}{A^2 + B^2}\right)^{\frac{1}{2}}e^{j\phi_{11}(\lambda)}$$

$$j\phi_{21}(\lambda)$$

$$A = \mu\lambda_1^4 - \lambda_1^2\left(l^2\lambda_2^2 + \mu\lambda_2^2 + 4\xi_1\xi_2\lambda_2^2l^2 + h^2\right) + l^2\lambda_2^2$$

$$B = \lambda_1^3\left(2\mu\xi_1 + 2\xi_1h^2 + 2\xi_2\lambda_2l^2\right) - \lambda_1\left(2\xi_2\lambda_2l^2 + 2\xi_1\lambda_1\lambda_2l^2\right)$$

$$D_{11} = \frac{h^2 + l^2\lambda_2^2 - \mu\lambda_1^2}{nk_1}$$

$$E_{11} = \frac{\lambda_1(2\xi_1h^2 + 2\xi_2l^2\lambda_2)}{nk_1} \tag{22}$$

$$D_{21} = \frac{h\lambda_1^2}{nk_1}$$

$$E_{21} = \frac{2j\lambda_1\xi_1}{nk_1}$$

$$H_{21}(\lambda_x) = \left|H_{21}(\lambda_x)\right|e^{j\phi_{21}(\lambda)} = \left(\frac{D_{21}^2 + E_{21}^2}{A^2 + B^2}\right)^{\frac{1}{2}}e \quad \phi_{11}(\lambda) = \arctan\frac{AE_{11} + BD_{11}}{AD_{11} - BE_{11}} \quad \phi_{21}(\lambda) = \arctan\frac{AE_{21} + BD_{21}}{AD_{21} - BE_{21}}.$$

The special solution to the first part of the differential equation can be expressed as follows:

$$\begin{cases} X_{11} = H_{11}(\omega_x)F_1 = p_k\left|H_{11}(\lambda)\right|\sin\left(\omega_x t + \theta_m + \phi_{11}(\lambda)\right), \\ \varphi_{21} = H_{21}(\omega_x)F_1 = p_k\left|H_{21}(\lambda)\right|\sin\left(\omega_x t + \theta_m + \phi_{21}(\lambda)\right). \end{cases} \tag{23}$$

In (22), $|h_{21}(\lambda)|$ and $|h_{22}(\lambda)|$ are the power amplification factors, and $\varphi_{21}(\lambda)$ and $\varphi_{22}(\lambda)$ are the phase factors.

Similarly, the special solution to the second part of the equation is as follows:

$$\begin{cases} X_{12} = H_{12}(\omega_z)e^{j\left(\omega_z t + \vartheta_i - \beta\right)}, \\ \varphi_{22} = H_{22}(\omega_z)e^{j\left(\omega_z t + \vartheta_i - \beta\right),} \end{cases} \tag{24}$$

where ω_z is the circular frequency and $\vartheta_i - \beta$ is the initial phase angle . $j^2 = 1$.

$$\begin{aligned} H_{12}(\lambda) &= \left|H_{12}(\lambda)\right|e^{j\phi_{12}(\lambda)} = \left(\frac{D_{12}^2 + E_{12}^2}{A^2 + B^2}\right)^{\frac{1}{2}} e^{j\phi_{12}(\lambda)}, \\ H_{22}(\lambda) &= \left|H_{22}(\lambda)\right|e^{j\phi_{22}(\lambda)} = \left(\frac{D_{12}^2 + E_{12}^2}{A^2 + B^2}\right)^{\frac{1}{2}} e^{j\phi_{22}(\lambda)}. \end{aligned} \tag{25}$$

Repeating the first part of the procedure yields the following:

$$\begin{cases} D_{12} = -\dfrac{h\lambda_1^2}{nk_1}, E_{12} = -2\lambda_1\xi_1/nk_1 \\ D_{22} = \dfrac{\left(1 - \lambda_1^2\right)}{nk_1}, E_{22} = 2\lambda_1\xi_1/nk_1 \\ \phi_{21}(\lambda) = \arctan\dfrac{AE_{12} + BD_{12}}{AD_{12} - BE_{12}}, \phi_{22}(\lambda) = \arctan\dfrac{AE_{22} + BD_{22}}{AD_{22} - BE_{22}}. \end{cases} \tag{26}$$

The special solution to the second part of the differential equation can be written as follows:

$$\begin{cases} X_{12} = H_{12}(\omega)F_2 = p_i l_i \zeta_i \left|H_{12}(\lambda)\right|\sin\left(\omega_z t + \vartheta_i + \phi_{12}(\lambda)\right) \\ \varphi_{22} = H_{22}(\omega)F_2 = p_i l_i \zeta_i \left|H_{22}(\lambda)\right|\sin\left(\omega_z t + \vartheta_i + \phi_{22}(\lambda)\right). \end{cases} \tag{27}$$

According to the superposition principle of the differential equation solution and by combining the above solution results, the final solution to the differential equation for the horizontal and rotational response forces of the multi-dimensional vibration isolator system is as follows:

$$\begin{cases} X = X_{11} + X_{12} = \sum_{m=1}^{n} p_m\left|H_{11}(\lambda)\right|\sin\left(\omega_x t + \theta_m + \phi_{11}(\lambda)\right) + \sum_{i=1}^{n} p_i l_i \zeta_i \left|H_{12}(\lambda)\right|\sin\left(\omega_z t + \vartheta_i + \phi_{12}(\lambda)\right) \\ \varphi = \varphi_{21} + \varphi_{22} = \sum_{m=1}^{n} p_m\left|H_{21}(\lambda)\right|\sin\left(\omega_x t + \theta_m + \phi_{21}(\lambda)\right) + \sum_{i=1}^{n} p_i l_i \zeta_i \left|H_{22}(\lambda)\right|\sin\left(\omega_z t + \vartheta_i + \phi_{22}(\lambda)\right), \end{cases} \tag{28}$$

where $h_{12}(\lambda) = h_{21}(\lambda)$; u_{cm} is the vertical vibration response at the center of the vibration isolator system; and l_i represents the horizontal distance from the other position points on the vibration isolator to the center point.

Equation (27) shows that when the vibration isolation system is under the action of nonuniform excitation, the horizontal vibration response of the vibration isolation system is affected by the common effect of horizontal excitation and vertical excitation; the rotation response of the VIP is also affected by the common effect of horizontal excitation and vertical excitation; and the vertical displacement response at different positions on the VIP system can be expressed as $Z = u_{\mathrm{cm}} \pm l_i\varphi$.

3. Parametric Dynamic Characterization of Vibration Isolator Systems

The vibration isolation performance is defined in terms of the logarithmic power amplification factor, $\beta(\lambda) = lg|h_i(\lambda)|$, where $\beta(\lambda)$ is the defined logarithmic power amplification factor and $|h_i(\lambda)|$ is the absolute value of the power amplification factor; only three power amplification factor parameters, $h_{11}(\lambda)$, $h_{12}(\lambda)$ and $h_{22}(\lambda)$, need to be discussed here.

3.1. Theoretical Analysis of the Stability Parameters of Vibration Isolator Systems. To improve the stability of the vibration isolation system and reduce the adverse effects caused by the rotation of the vibration isolation system, the factors affecting the stability of the VIP system, such as the length of the VIP, the number of vibration isolator arrangements and the location of the horizontal vibration isolator arrangement, are analyzed.

3.1.1. Effect of the Length of the Vibration Isolator on the Stability of the Vibration Isolator System. The following fixed parameters were set for analysis: $N = 2$, $h = 0.2$ m, $\xi_1 = 0.065$, $\xi_2 = 0.05$, and $\lambda_2 = 1.5$. With the above-fixed parameters set, four working conditions were considered with vibration isolators of lengths $l = 3$ m, 5 m, 10 m, and 20 m. The variation in the logarithmic power amplification coefficient under different vibration isolator lengths is shown in Figure 3 below.

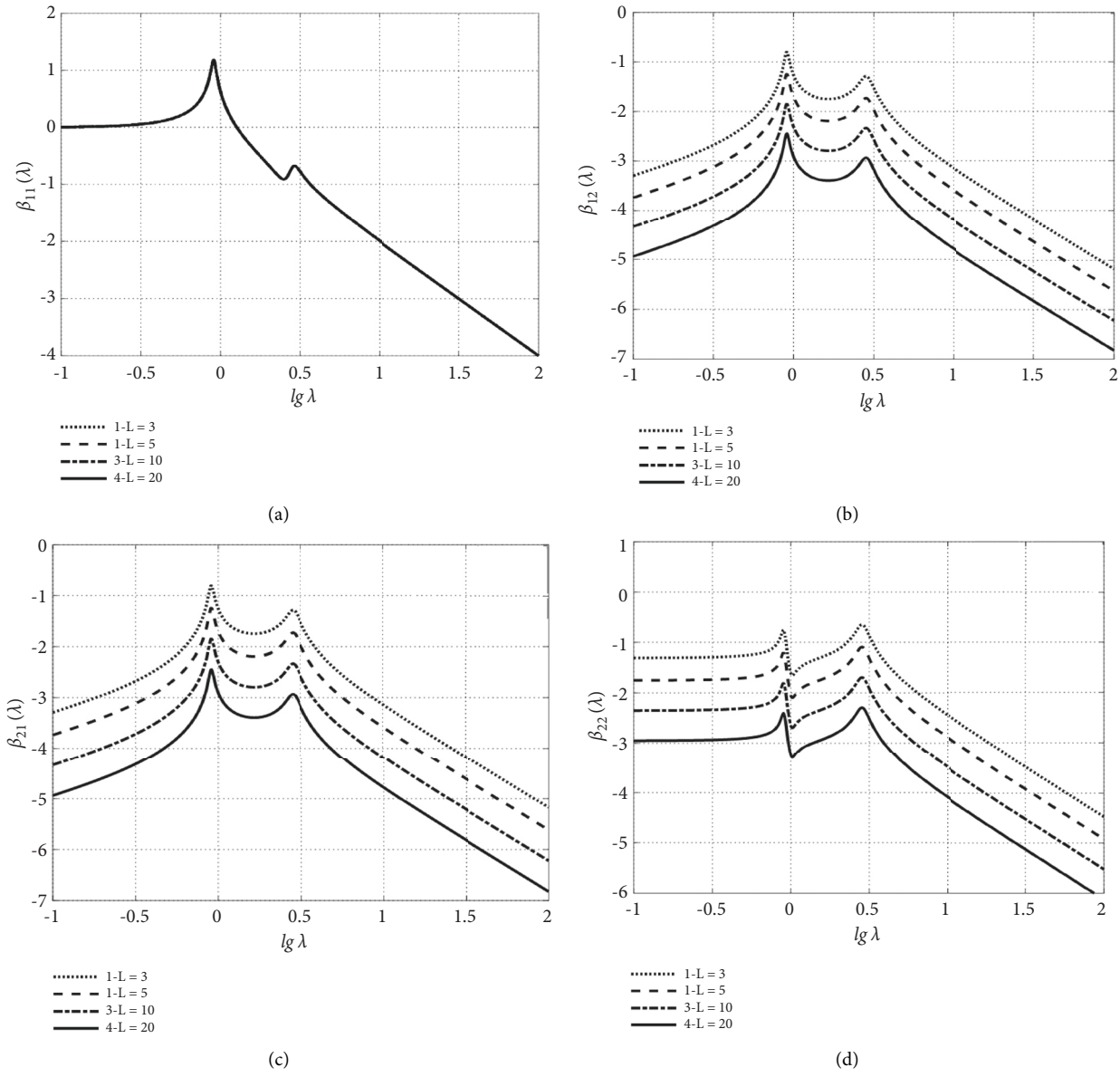

Figure 3: Logarithmic dynamic amplification factor under different vibration slab length changes.(a) logarithmic dynamic amplification factor β_{11} (b) logarithmic dynamic amplification factor β_{12}.(c) logarithmic dynamic amplification factor β_{21} (d) logarithmic dynamic amplification factor β_{22}.

Figure 3(a) shows that the logarithmic dynamic amplification factor β_{11} remains the same as the length of the vibration isolator increases; Figure 3(b)–3(d) show that the logarithmic dynamic amplification factors β_{12}, β_{21}, and β_{22} decrease as the length of the vibration isolator increases. This means that as the length of the vibration isolator increases, the rotation response of the vibration isolation system decreases, and the vibration isolator system is less affected by its own rotation; the horizontal vibration of the vibration isolator is less affected by the rotation of the system.

3.1.2. Effect of the Number of Vibration Isolator Arrangements on the Stability of the Vibration Isolator System. The fixed parameters set are as follows: $l = 3$ m, $h = 0.2$ m, $\xi_1 = 0.065$, $\xi_2 = 0.05$, and $\lambda_2 = 1.5$. Based on the fixed-parameter set, the number of vibration isolators arranged under the platform is considered to be $N = 2$, 4, 6, and 8 for the four working conditions. The variation law of the logarithmic dynamic amplification coefficient under different numbers of vibration isolators is shown in Figure 4.

Figure 4(a) shows that with the increase in the number of spring isolators of the vibration isolation system, the logarithmic dynamic amplification coefficient β_{11} remains stable; Figures 4(b), 4(c) and 4(d) shows that with the increase in the number of spring isolators in the vibration isolation system, the logarithmic dynamic amplification coefficients

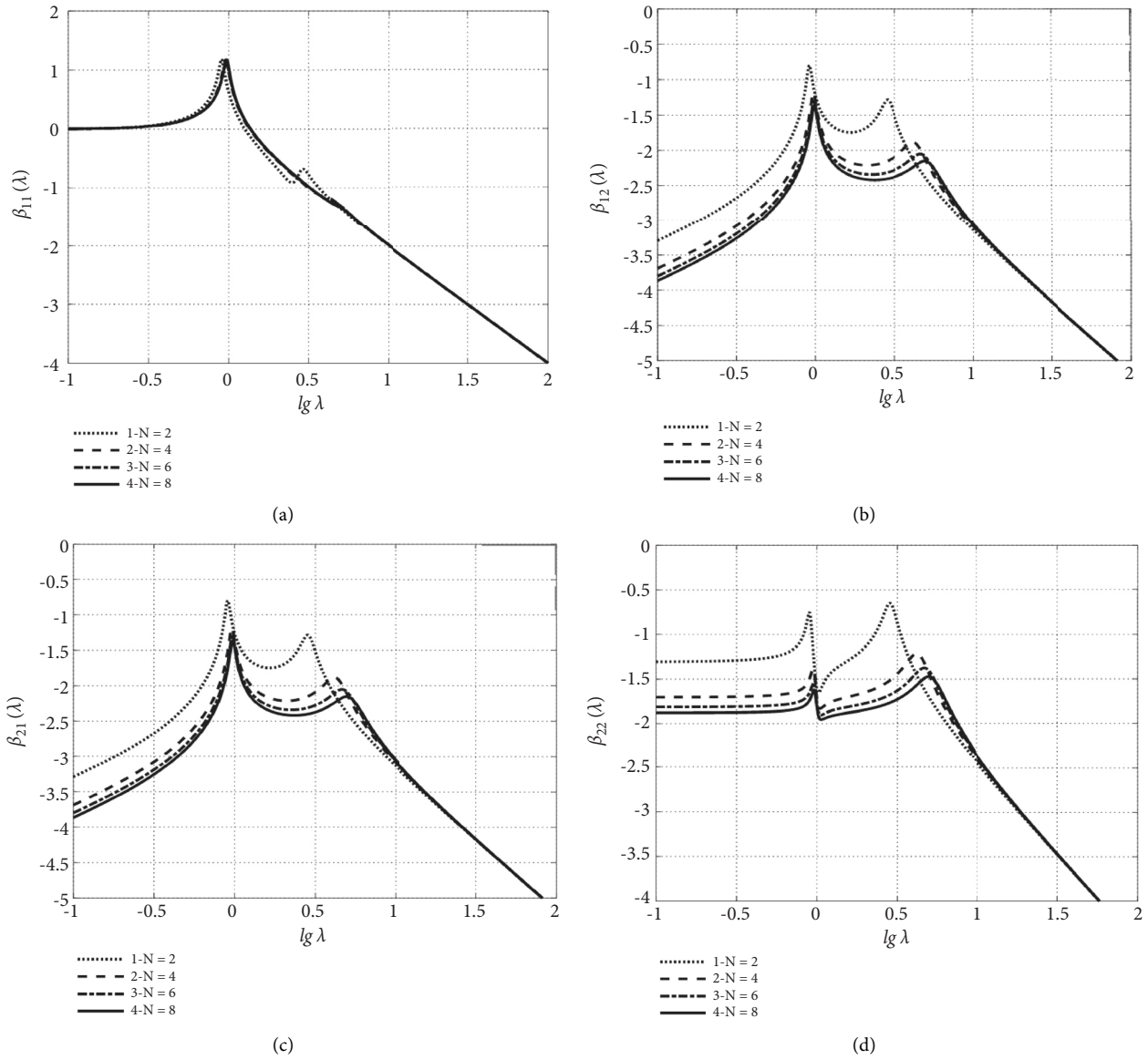

Figure 4: The variation law of the logarithmic dynamic amplification coefficient under different numbers of vibration isolators: (a) logarithmic dynamic amplification factor β^{11},(b) logarithmic dynamic amplification factor β^{12}, (c) logarithmic dynamic amplification factor β_{21}, and (d) logarithmic dynamic amplification factor $\beta_{2.}$

β_{12}, β_{21} and β_{22} gradually decrease. With the increase in the number of isolators, the rate of decrease in the logarithmic dynamic amplification coefficient gradually decreases. As a result, the horizontal response of the vibration isolation system is less affected by the rotation of the vibration isolator, and the impact on the stability of the VIP system is also gradually reduced.

3.1.3. Effect of the Position of the Horizontal Vibration Isolator on the Stability of the Vibration Isolation Plate System. The fixed parameters are set as follows: $l = 3$m, $\xi_1 = 0.065$, $\xi_2 = 0.05$, $\lambda_2 = 1.5$, and $N = 2$. Based on the fixed parameters, four working conditions are considered for the horizontal vibration isolator position: $h = 0.2$ m, 0.5 m, 0.8 m, and 1.0 m. The variation law of the logarithmic power amplification coefficient under different horizontal vibration isolator arrangement positions is shown in Figure 5.

Figure 5(a) shows the logarithmic power amplification coefficient. β_{11} does not change as the value of h increases. Figure 5(b) and 5(c) shows that β_{12} increases as the value of h increases. Figure 5(d) shows that β_{22} changes in a three-step pattern as h increases: before the first peak point, β_{22} increases as the value of h increases, after the second peak point, β_{22} increases as the value of h value increases, after the second peak point, β_{22} decreases with the increase in h value, and after the third peak point, β_{22} tends to be the same. Thus, considered together, reducing the value of the horizontal vibration isolator position h reduces the rotational response of the vibration isolator.

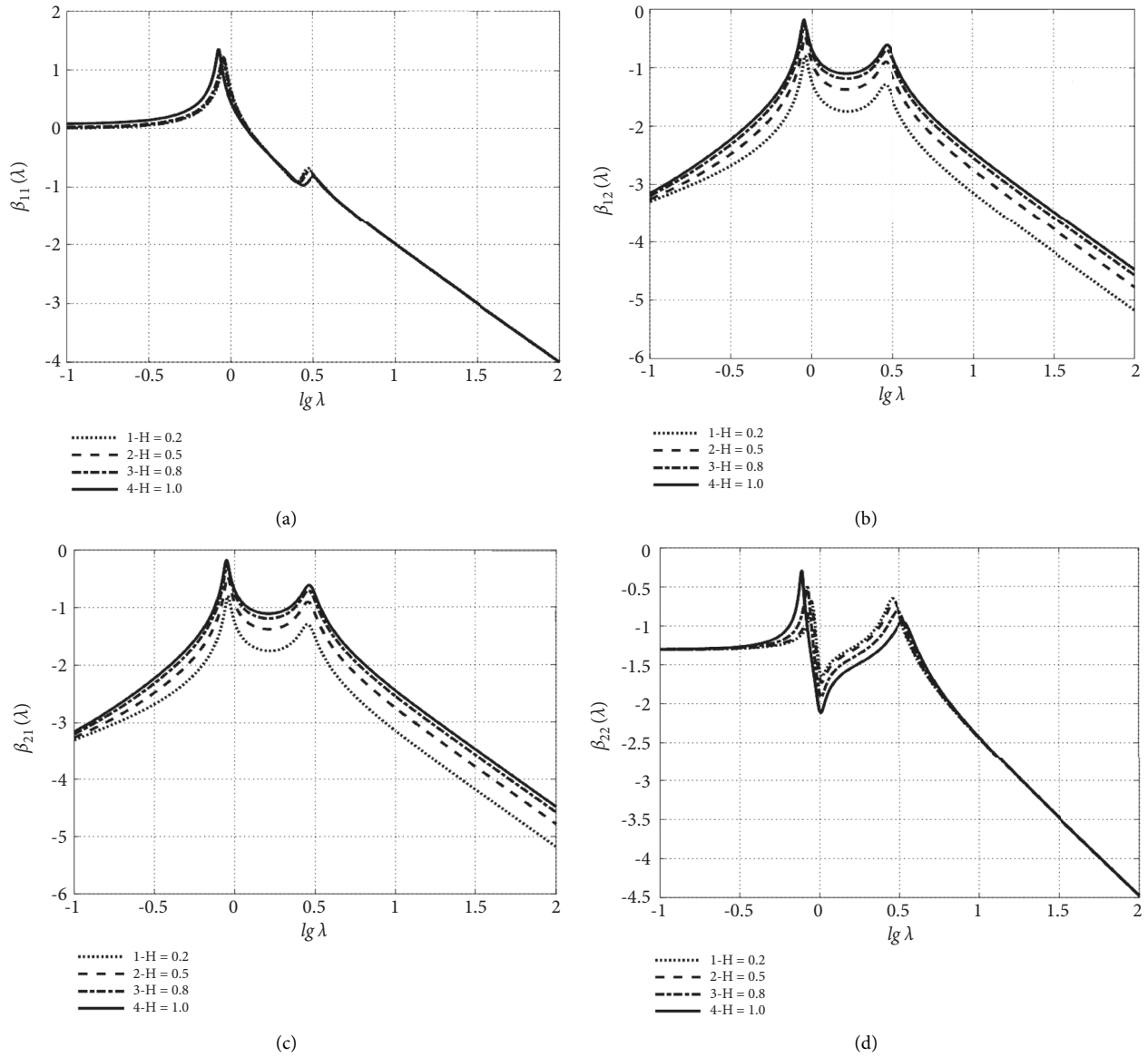

Figure 5: The variation law of the logarithmic power amplification coefficient under different horizontal vibration isolator arrangement positions: (a)logarithmic dynamic amplification factor $\beta_{11,}$ (b)logarithmic dynamic amplification factor β_{12}, (c)logarithmic dynamic amplification factor β_{21}, and (d)logarithmic dynamic amplification factor $\beta_{22.}$

Among the above parameters, the logarithmic power amplification coefficient β_{11} is unaffected; β_{21} and β_{22} decrease with the increase in the length of the VIP system and decrease with the increase in the number of spring vibration isolators; β_{21} increases with the increase in the horizontal vibration isolator position h value, and β_{22} shows a three-stage change form of first increasing, then decreasing, and finally keeping no edge with the increase in h value.

4. Verification of the Numerical Analysis of the Vibration Isolator System

A numerical model of the VIP is established to transiently analyze the vibration of the VIP system under the action of simple harmonic excitation. A finite-element model of the vibration isolator system is established, as shown in Figure 6. To simplify the analysis process, only the numerical simulation of the vibration of the VIP in the vertical and horizontal X directions is considered.

The model consists of a VIP, spring vibration isolators and a base platform, from top to bottom. The VIP has a length of 6 m, a thickness of 10 cm, a width of 3 m, a density of $\rho = 2700\,\text{kg/m}^3$, and a modulus of elasticity $E = 3.0 \times 10^{10}\,\text{Pa}$. The bottom and ends of the vibration isolator (X direction) are evenly arranged with different numbers of spring vibration isolators according to the study conditions, and the horizontal isolators are at the same height as the center of gravity of the VIP. The spring stiffness of the isolator is $8 \times 10^6\,\text{N/m}$, and the damping coefficient is 0.05. The ShELL63 unit is used to simulate the VIP unit, and

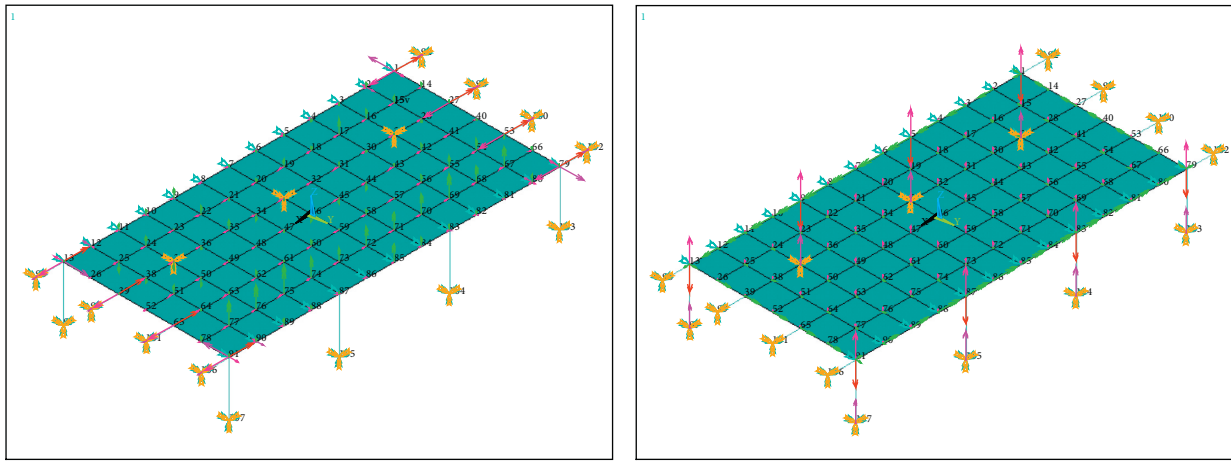

Figure 6: Finite element model of vibration isolation system.

a COMBIN14 unit is used to simulate the spring isolator unit, with the boundary conditions set with all constraints at the bottom of the base plate, all constraints set on both sides of the horizontal X direction of the VIP, and only DY constraints set on both sides of the horizontal Y direction of the VIP.

The frequency f_i values taken in this study are 1 Hz, 5 Hz, and 15 Hz at low frequencies, and the load excitation used in the numerical simulation is 800 N. The fitted load is loaded onto the model with an integration step of 0.005 s to obtain the vibration response of the vibration isolator system at different pickup points.

4.1. Vertical Response of a Vibration Isolator System under Uniform Excitation. Assuming that the initial phase of the simple harmonic excitation load is 0, the fixed parameters are set as follows: the horizontal and vertical directions of the VIP are uniformly arranged with eight vibration isolators, the horizontal vibration isolators are arranged with the center of gravity of the VIP at the same height, the damping ratio of the vibration isolators is 0.05, the spring stiffness is 8.0 MN/m, the thickness of the VIP is 10 cm, the support distance is 3@2 m, and the external excitation is assumed to be applied to the VIP by the arranged vertical vibration isolators. Comparing the vibration isolator to the VIP, the results are shown in Figure 7 and Table 1.

Figure 7 shows the vibration response of the vibration isolator system at 1, 5, and 15 Hz under simple harmonic excitation conditions through ANSYS numerical simulation and theoretical derivation of the vibration pickup point. The figure shows that the time course curve of the vertical acceleration at the pickup point obtained from the numerical simulation and the time course curve obtained from the theoretical derivation are basically the same, and Table 1 shows that the data obtained from the numerical simulation and the theoretical derivation are also very close to each other, which verifies the accuracy of the theoretical derivation.

Table 1 shows that the external excitation frequency of 1, 5, and 15 Hz, and the difference between the simulated values and the theoretically derived results gradually increase. As this study focuses on the vibration isolation characteristics of the VIP system under the low-frequency vibration response of the building floor caused by a train, the numerical simulation is still able to simulate the vibration of the VIP more accurately.

5. Vibration Isolation Analysis of VIP Systems under the Action of Running Trains

By establishing a three-dimensional finite element model of the train-track-soil-building-VIP system, the vibration isolation effect of the floor VIP system under train operation and the effect of structural parameter changes on the vibration isolation of the floor VIP are analyzed in two ways. The whole model is divided into two subsystem models for the convenience of calculation, i.e., the train-roadbed model and the foundation soil-buildings-VIP system model. As the building floor is dominated by vertical vibration [16], this study only analyses the vertical vibration isolation of the vibration platform system.

5.1. Train-Track System Model. The dynamic analysis model of the train-track system consists of the vehicle model and the track model, which are in line with the Hertz wheel-rail contact relationship. During the operation of the train, the moving axle weight produces both vertical and lateral forces on the bottom roadbed, and the vertical action is much larger than the lateral action; thus, only the vertical vibration needs to be considered in the analysis process, and the lateral vibration is ignored.

5.1.1. Train Models. A model train is normally made up of several locomotives. Each locomotive is a multi-degree-of-freedom vibration system consisting of a body, a bogie, a wheel-set, two-series springs, and dampers. Each locomotive and bogie has only two degrees of freedom, nod, and float, and the center of gravity of the locomotive is

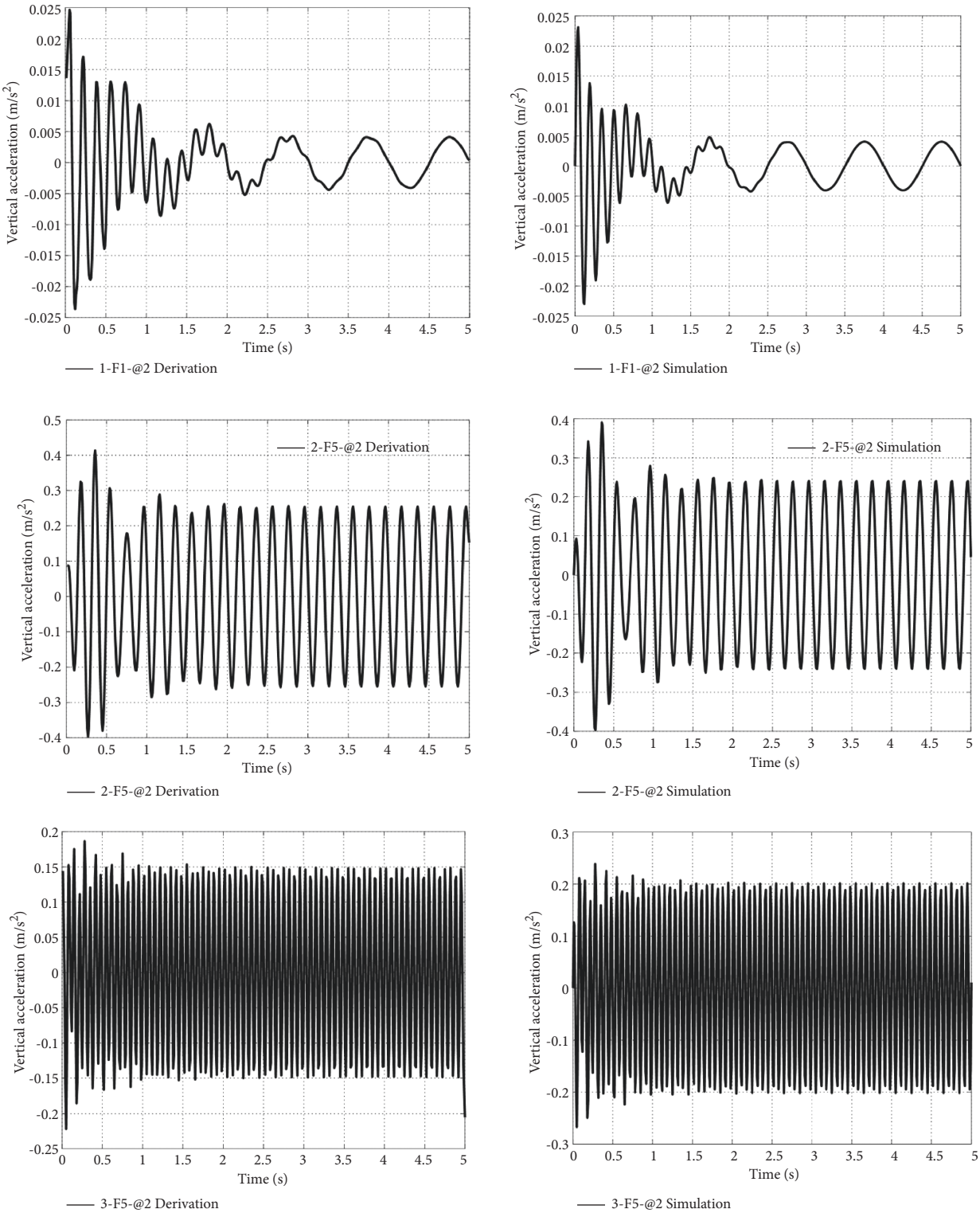

Figure 7: Comparison of theoretical derivation and numerical analysis of vibration point under multi-point excitation.

represented by the coordinates Z_c and φ_c; the center of gravity of the body is represented by the coordinates Z_T and φ_T; and the wheel pair has only one degree of freedom, which can be represented by Z_W.

5.1.2. Track Model. The rail model as a whole can be considered a triple mass-spring damper system. The main components of the system are the rail, plastic mat, rail sleeper, and bed reference mass. The rail is assumed to be an

Table 1: Comparison of simulation results and theoretical derivation of points under different frequency excitations.

External excitation frequency (Hz)	Displacement ($\times 10^{-4}$m)		Point acceleration($\times 10^{-1}$ m/s^2)		Vibration level(dB)	
	Numerical simulation	Theoretical derivation	Numerical simulation	Theoretical derivation	Numerical simulation	Theoretical derivation
1	1.036	1.024	0.0437	0.0406	72.81	72.17
5	2.677	2.447	2.578	2.426	108.23	107.70
15	0.233	0.235	1.500	2.028	103.52	106.14

Table 2: Soil properties.

Type of soil	Depth(m)	Modulus of elasticity/Mpa	Poisson's ratio	Damping ratio	Density/Kg/m^2	Shear wave speed s/m·s^{-1}	Compression wave speed s/m·s^{-1}
Mixed fill	1	191	0.36	0.03	1980	203	411
Powdered clay	3	268	0.33	0.03	1990	216	475
Coarse sand	4	394	0.23	0.03	1918	260.2	416.0
Gravelly sand	32	430	0.29	0.03	2122	351.8	879.5

infinitely long beam on elastic supports, but a suitable length is chosen for the specific analysis. In the numerical analysis, the mass of the rail forms the nodal mass matrix M_r in the finite element, the stiffness forms the nodal stiffness matrix K_r in the finite element, and the damping matrix can be represented by the Riley damping $Cr = \alpha M_r + \beta K_r$. A rail node has two degrees of freedom, i.e., vertical and corner, and one vertical displacement degree of freedom at each elastic support point. The rail system dynamics parameters are detailed in the literature [20].

5.2. Finite Element Model of the Soil-Building-Vibration Isolator System

5.2.1. Soil Model. Vibrations and microvibrations of the soil caused by rail traffic, the soil strain, are treated as an elastic deformation phase; the effect of nonlinear factors in the soil material is not considered.

The dimensions of the model are set as follows: the width of the foundation is 140 m in the vertical X direction of the track, the length of the foundation is 100 m along the Y direction of the track, and the depth of the foundation soil h is 40 m. The model soil parameters are shown in Table 2 below.

The simulated boundary is an artificial viscoelastic boundary, which is implemented by arranging the spring and damping system on the truncated boundary of the soil model, taking the form in (28):

$$\begin{cases} K_{BT} = \alpha_T \dfrac{G}{R}, C_{BT} = \rho c_s \\ \\ K_{BN} = \alpha_N \dfrac{G}{R}, \quad C_{BN} = \rho c_p \end{cases}, \tag{29}$$

where K_{BT} and K_{BN} represent the spring normal stiffness and tangential stiffness, respectively; R is the distance from the wave source to the artificial boundary; c_s and c_p represent the shear and compressional wave velocities in the medium, respectively; G is the medium shear modulus; ρ is the density of the foundation soil; α_T and α_N represent the tangential and normal viscoelastic artificial boundary parameters, respectively; and the damping ratio $\xi_0 = 0.03$ in the soil body.

5.2.2. Finite Element Model of the Soil-Building-Vibration Isolator System. The building is a 12-story cast-in-place reinforced concrete frame structure, and the column network arrangement is shown in Figure 8 below. The building has 12 stories above ground with a floor height of 3 m and 1 story below ground with a floor height of 4 m. The column cross-sectional dimensions of the 1st to 4th stories are 600×600 mm, with a main beam cross-section of 350×600 mm and a secondary beam cross-section of 250×400 mm; the column cross-sectional dimensions of the 5th to 12th stories are 500×500 mm, with a main beam cross-section and secondary beam cross-section of 250×400 mm.

According to the design plan, the frame structure has a horizontal longitudinal three-span structure of 6 m-2 m-6 m dimensions, and the length of all seven openings along the horizontal transverse direction is 6 m. The building frame beams, columns, floor slabs, and continuous underground walls are all made of C30 concrete with a modulus of elasticity of 30 kN/mm^2 and a reinforced concrete material with a density of $\rho = 2700$ kg/m^3. The basement uses a box-shaped foundation with a basement floor slab of 400 mm and walls that are 180 mm thick.

The VIP system is set at the mid-span of each floor of the building. The finite element model parameters are as follows: a platform length of 6 m, a thickness of 0.1 m, a platform width of 3.0 m, several vibration isolators arranged under the plate, a density ρ of 2700 kg/m^3, and a concrete strength of C30; the VIP is simulated using SHELL63 units, and spring vibration isolators are simulated using COMBIN14 units. The modulus of elasticity of the platform is $E = 3.0 \times 10^{10}$ Pa, the vertical stiffness of the spring is $K = 8.0 \times 10^6$ N/m, and the damping ratio coefficient is 0.05.

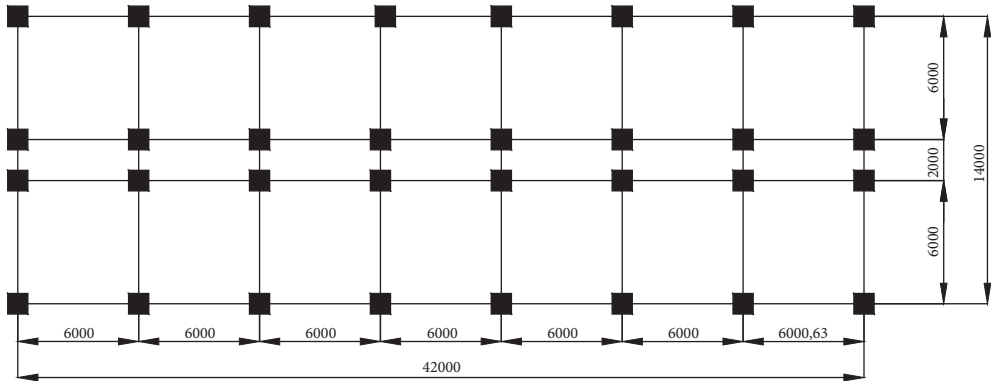

Figure 8: The schematic diagram of building plane (mm).

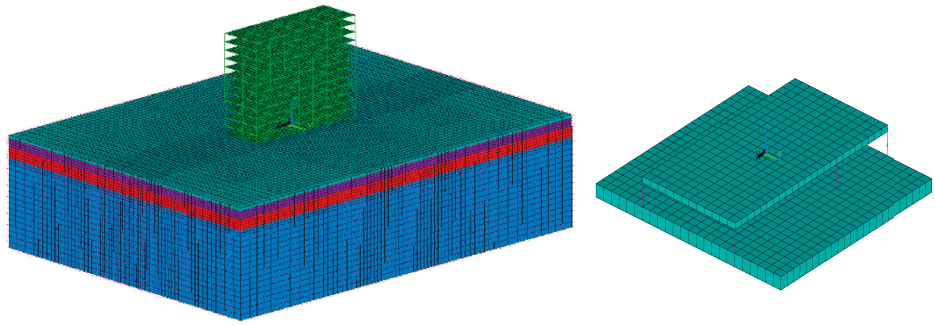

Figure 9: Soil-building-isolation slab finite element model.

The soil-building contact surfaces in this study mainly take the form of coordinated deformation contacts. The three-dimensional finite element model of the foundation soil-contact surface-building-vibration isolator interaction is shown in Figure 9.

5.3. Vibration Isolation Analysis of a VIP under the Action of Running Trains

5.3.1. Train Load Simulation. The train type is CRH2 rolling stock, and the CRH2 single-section vehicle parameters are detailed in the literature [4]. The train-track model program was used to input the parameters of this type of train and then obtain the wheel-track excitation loads for two operating conditions of 90 km/h and 150 km/h, as shown in Figure 10. Then, the excitation is input into the soil-building finite element model, and the vibration acceleration level VL is used as the evaluation criterion for building vibrations.

5.3.2. Comparative Analysis of the Vibration Responses of a Building Floor System with and without Vibration Isolators. The fixed parameters are set, and the working conditions are as follows: the train speed is 150 km/h, eight vibration isolators are evenly arranged under the platform, the spring stiffness is 0.2 MN/m, the vibration isolator damping ratio is 0.05, the thickness of the VIP is 10 cm, the support distance is 3@2 m, the VIP size is kept the same as above, and the distances between the train vibration source and the building are 15 m, 21 m and 27 m for the three working conditions. Due to space limitations, the vertical vibration responses of the first floor of the building with and without the VIP are only studied in this study, as shown in Figure 11.

Figure 12 shows the time courses of acceleration at the pickup point for the first floor of the building with and without vibration isolators at different source distances (15 m, 21 m, and 27 m) and train speeds of 150 km/h·m/s^2.

The acceleration time domain analysis shown in Figure 12 and Table 3 shows that the vibration isolation efficiency of the vibration isolation system for the acceleration response can reach approximately 85%, and the vibration isolation efficiency of the VIP system for the floor vibration response is not affected by the vibration source distance. Therefore, considered together, the VIP system is suitable for vibration isolation of low-frequency vibrations of building floors caused by trains, and the vibration isolation effect is very significant.

5.4. Influence of VIP Structural Parameters on the Vibration Isolation Effect. Variations in the structural parameters of vibration isolators, such as the number of isolators, spring stiffness, isolator damping, thickness and other parameters, affect the vibration isolation effect. The vibration response of the vertical pickup point on the first floor of the building is analyzed for two vehicle speeds of 90 km/h and 150 km/h.

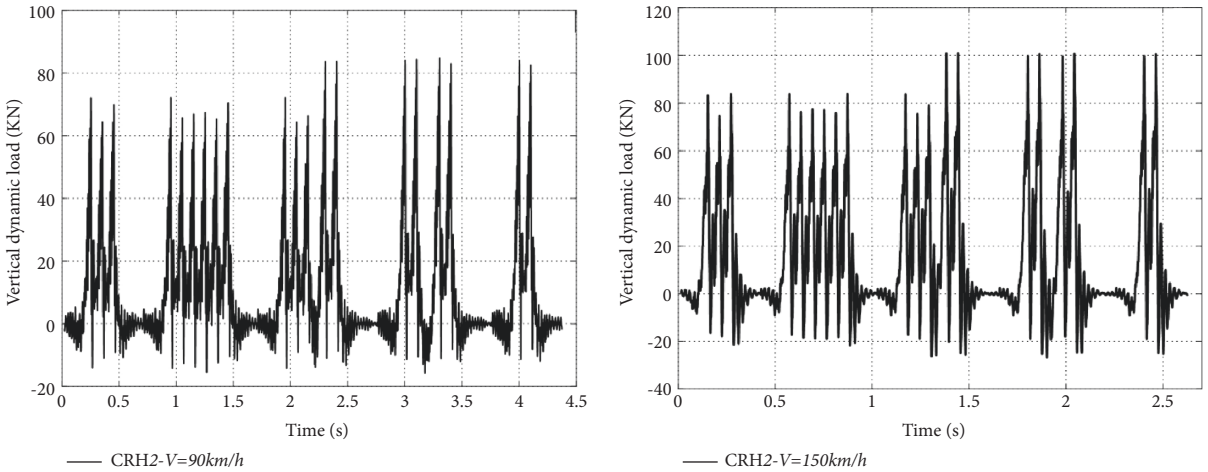

Figure 10: Wheel-rail excitation histories at different vehicle speeds.

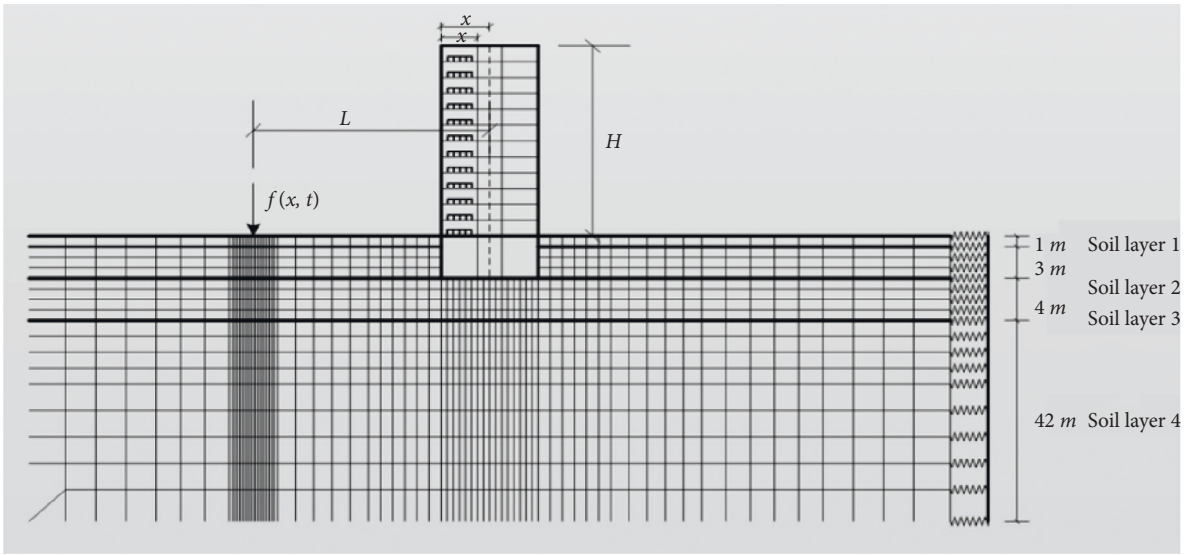

Figure 11: Schematic diagram of soil-building-isolation slab finite element analysis grid.

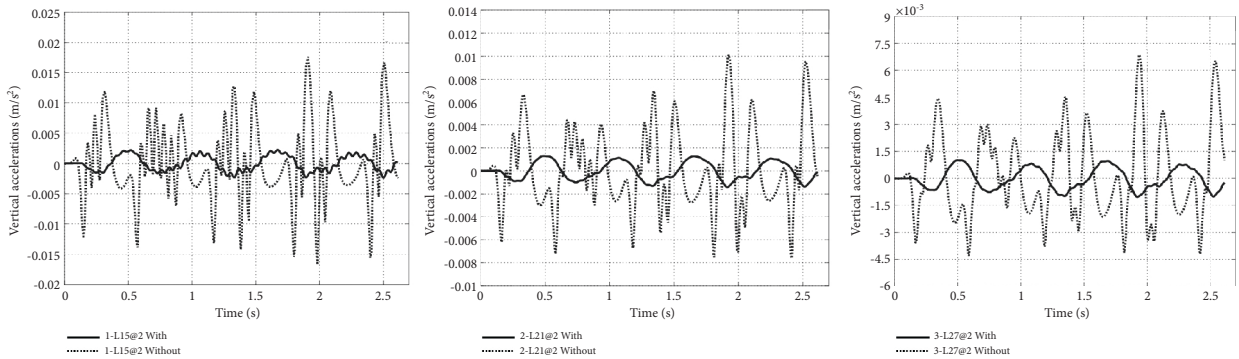

Figure 12: Vertical vibration isolation of the vibration isolation slab system 15m, 21m, and 27m from the center.

Table 3: Vibration comparison with and without vibration isolation system in different source distances.

Vibration source distance	(l = 15 m)			(l = 21 m)			(l = 27 m)		
(Before/After) isolation	Before	After	T_r(%)	Before	After	T_r(%)	Before	After	T_r(%)
Acceleration($\times 10^{-3}$ m/)	17.620	2.390	13.56	10.122	1.409	13.92	6.56	1.023	14.92

Table 4: Number of vibration legislators conditions.

Condition number	Cases	Isolator thickness H(cm)	Support distance S(m)	Spring stiffness $k(MN/m)$	Number of isolators
1	N4@6	10	1@6	0.2	4
2	N8@2	10	3@2	0.2	8
3	N16@1	10	6@1	0.2	14

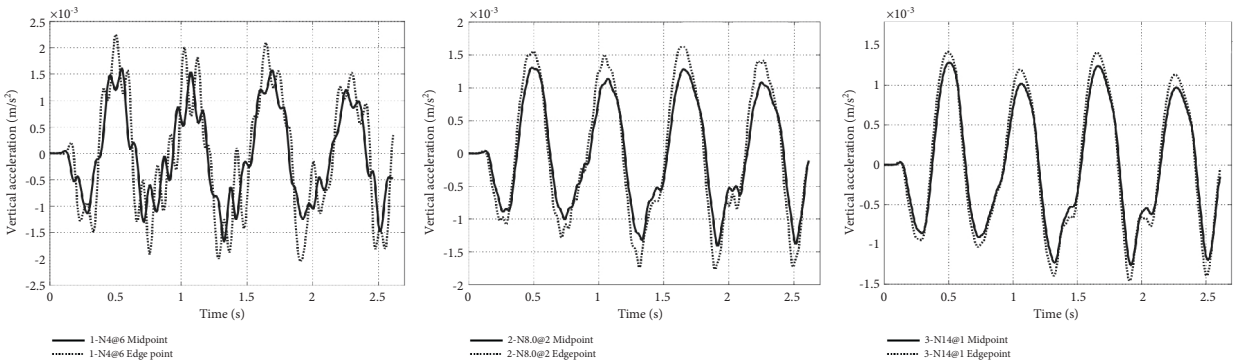

Figure 13: Vertical acceleration response of different pickup points when the number of isolators changes.

5.4.1. Influence of the Number of Vibration Isolators. Setting the fixed parameters shown in Table 4, the number of vibration isolators is $N = 4$, 8, 14. Figure 13 shows the acceleration time range of the vibration isolator center pickup point and edge pickup point under the three working conditions.

Figure 13 shows that when the number of isolators increases, the acceleration response at the midpoint and edge points of the vibration isolator decreases. An increase in the number of isolators is beneficial to reducing the vibration isolator acceleration response, but the reduction effect is less obvious.

5.4.2. Steel Spring Stiffness Effects. The damping coefficient of the vibration isolator is 0.05, the thickness of the vibration isolator is 10 cm, the vibration isolator distance is 3.0 m, and the vertical stiffness of the spring is $K = 0.32$ MN/m.

The results can be seen in Figure 14. When the spring stiffness increases, the acceleration response of the vibration isolator gradually increases. however, the change in spring stiffness has a greater effect on the vibration response of the vibration isolator; when the spring stiffness of the vibration isolator is beyond a specific range, the vibration of the vibration isolator is accompanied by an increase in vibration and acceleration response. When the spring stiffness of the vibration isolator exceeds a specific range, not only is there no vibration isolation effect, but there may also be a slight "amplification" phenomenon.

5.4.3. Effect of the Vibration Isolator Damping Ratio. The employed train speeds are 90 km/h and 150 km/h. Eight vibration isolators are arranged under the slab, and the spring stiffness of the vibration isolators is 0.6 M, the thickness of the vibration isolators is 10 cm, and the vibration isolation distance is 2.0 m. The damping ratios of the vibration isolators are set to 0.01, 0.05, 0.10, and 0.15. The damping ratio of the concrete vibration isolator is 0.05. The acceleration time range curve and spectrum curve of the vibration pickup point of the vibration isolator on the first floor of the building with different vibration isolator damping ratios are shown in Figure 15.

As shown in Figure 15, as the damping ratio increases, the time it takes for the vibration isolator system response to reach the steady state decreases, and the vibration decay time of the vibration isolator decreases as the damping ratio increases.

5.4.4. Effect of Vibration Isolator Thickness. The employed train speeds are 90 km/h and 150 km/h, with eight vibration isolators arranged under the platform. The vibration isolator damping coefficient is 0.05, and the spring stiffness is 0.2 MN/m. The thicknesses of the VIP re $h = 10$ cm, 15 cm,

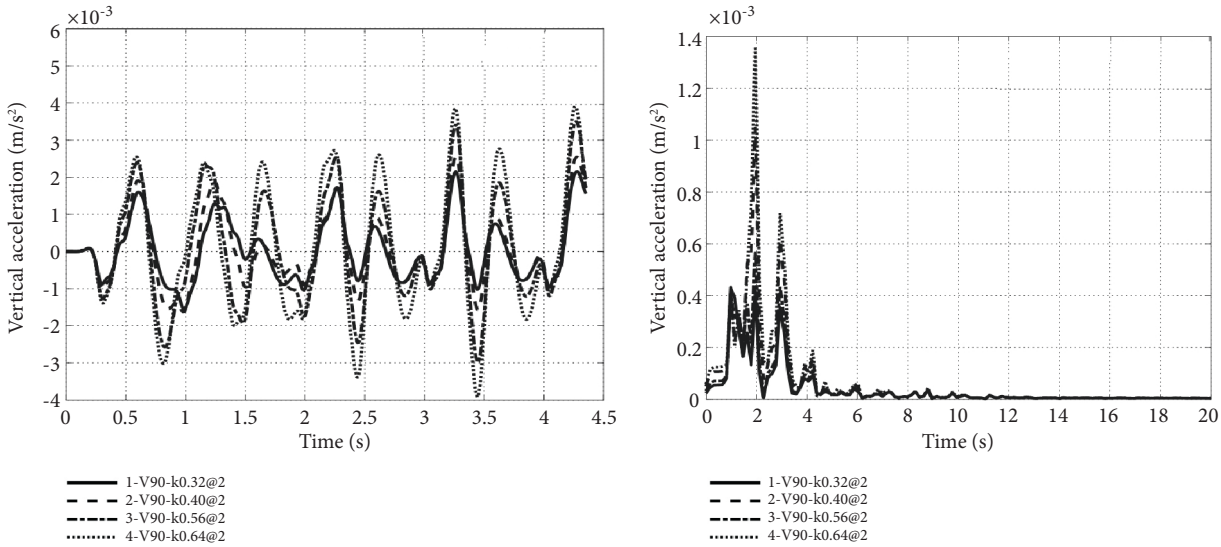

Figure 14: Vertical acceleration response of vibration pickup point under change of spring stiffness.

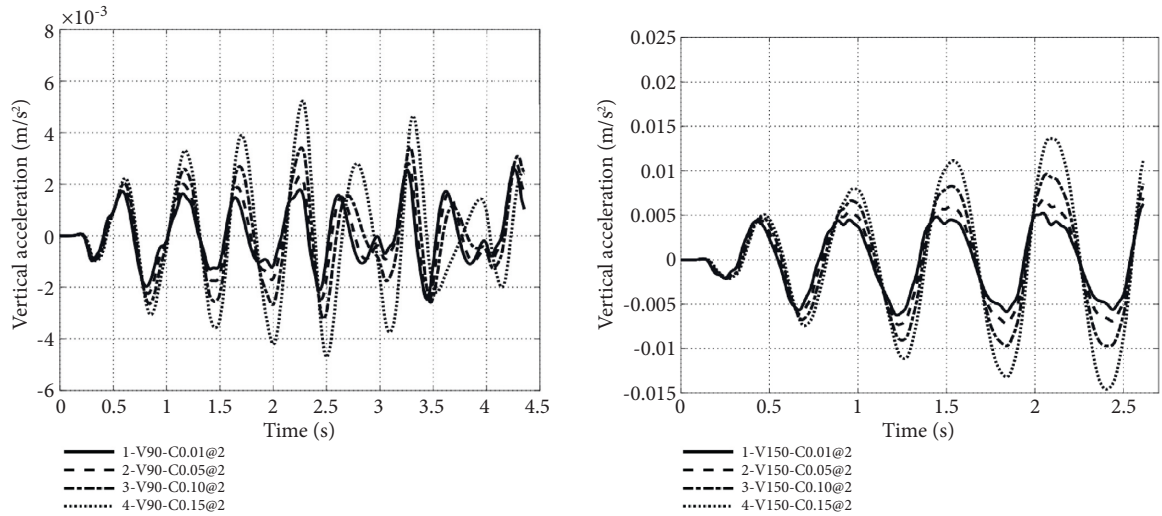

Figure 15: Vertical acceleration response of pickup point under change of damper ratio of vibration isolator.

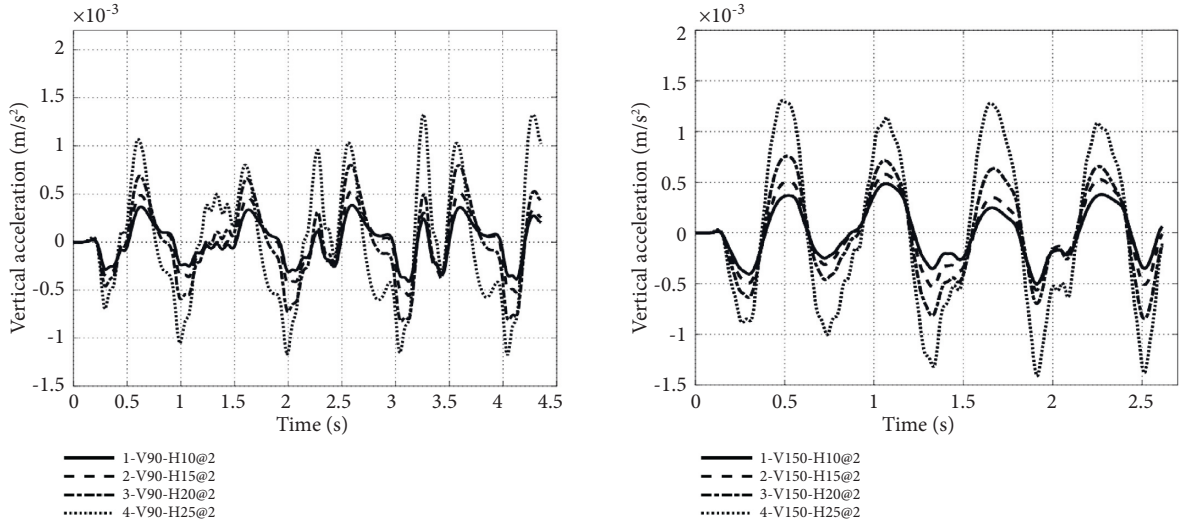

Figure 16: Vertical acceleration response of pickup point under thickness change of vibration isolation slab.

20 cm, and 25 cm for the four working conditions. Figure 16 shows the acceleration time curve at the pickup point of the vibration isolator on the first floor of the building with different vibration isolator thicknesses.

As shown in Figure 16, as the thickness of the vibration isolator increases, the acceleration response of the vibration isolator decreases, and the reduction is noticeable, which shows that increasing the thickness of the vibration isolator can reduce the vibration response of the vibration isolator more comprehensively.

6. Conclusions

This study focused on vibration isolation measures for building floor vibrations caused by running trains. Both theoretical derivation and numerical simulation were performed in this research, and the following conclusions were drawn. (1) The theoretical derivation and numerical analysis verified that the vibration response prediction model established in this study was feasible for the VIP system under the action of multi-point excitation. (2) Appropriate measures, such as increasing the number of vibration isolators, increasing the length of the vibration isolators and arranging the horizontal vibration isolators and the center of gravity of the vibration isolators at the same height, effectively improved the stability of the vibration isolator system. (3) VIP systems [21] were very effective [22] in reducing the [23] vibration of building floors caused by trains, and increasing the vibration isolator damping ratio and platform thickness and reducing the spring stiffness increasing the vibration isolation effect. (4) Variations in the distance between the running train and the building had a small effect on the vibration isolation efficiency of the secondary vibration response at the floor level.

Data Availability

The data that support the findings of this study are available from the corresponding author upon reasonable request.

Conflicts of Interest

No conflict of interest exists in the submission of this manuscript.

Acknowledgments

This research was supported by National Natural Science Foundation of China (52178101).

References

[1] L. Fang, J. Yao, and H. Xia, "Prediction on soil-ground vibration induced by high-speed moving train based on artificial neural network model," *Advances in Mechanical Engineering*, vol. 11, no. 5, Article ID 168781401984729, 2019.

[2] X. Sheng, C. J. C. Jones, and D. J. Thompson, "Prediction of ground vibration from trains using the wavenumber finite and boundary element methods," *Journal of Sound and Vibration*, vol. 293, no. 3-5, pp. 575–586, 2006.

[3] D. J. Thompson and C. J. C. Jones, "A review of the modelling of wheel/rail noise generation," *Journal of Sound and Vibration*, vol. 231, no. 3, pp. 519–536, 2000.

[4] J. Yao, R. Zhao, N. Zhang, and D. Yang, "Vibration isolation effect study of in-filled trench barriers to train-induced environmental vibrations," *Soil Dynamics and Earthquake Engineering*, vol. 125, 2019.

[5] E. E. Ungar, S. Dh, and C. H. Amick, "Vibration control design of high-technology facilities," *Sound and Vibration*, vol. 24, no. 7, pp. 20–27, 1990.

[6] J. S. hwang, Y. N. huang, Y. H. Hung, and J. C. huang, "Applicability of seismic protective systems to structures with vibration-sensitive equipment," *Journal of Structural Engineering*, vol. 130, no. 11, pp. 1676–1684, 2004.

[7] Y. L. Xu, H. J. Liu, and Z. C. Yang, "Hybrid platform for vibration control of high-tech equipment in buildings subject to ground motion. Part 1: experiment," *Earthquake Engineering & Structural Dynamics*, vol. 32, no. 8, pp. 1185–1200, 2003.

[8] Y. L. Xu and B. Li, "Hybrid platform for high-tech equipment protection against earthquake and microvibration," *Earthquake Engineering & Structural Dynamics*, vol. 35, no. 8, pp. 943–967, 2006.

[9] Y. Xu and A. X. Guo, "Microvibration control of coupled high tech equipment-building systems in vertical direction," *International Journal of Solids and Structures*, vol. 43, no. 21, pp. 6521–6534, 2006.

[10] Y. L. Xu, Z. F. Yu, and S. Zhan, "Experimental study of a hybrid platform for high-tech equipment protection against earthquake and microvibration," *Earthquake Engineering & Structural Dynamics*, vol. 37, no. 5, pp. 747–767, 2008.

[11] J. J. Yang, S. Y. Zhu, W. Zhai et al., "Prediction and mitigation of train-induced vibrations of large-scale building constructed on subway tunnel," *Science of the Total Environment*, vol. 668, pp. 485–499, 2019.

[12] R. A. Ibrahim, "Recent advances in nonlinear passive vibration isolators," *Journal of Sound and Vibration*, vol. 314, no. 3-5, pp. 371–452, 2008.

[13] I. F. Lazar, S. A. Neild, and D. J. Wagg, "Using an inerter-based device for structural vibration suppression," *Earthquake Engineering & Structural Dynamics*, vol. 43, no. 8, pp. 1129–1147, 2014.

[14] D. De Domenico and G. Ricciardi, "An enhanced base isolation system equipped with optimal tuned mass damper inerter (TMDI)," *Earthquake Engineering & Structural Dynamics*, vol. 47, no. 5, pp. 1169–1192, 2018.

[15] Y. A. Yun and Y. M. Li, "Design and analysis of a novel 6-DOF redundant actuated parallel robot with compliant hingesfor high precision positioning," *Nonlinear Dynamics*, vol. 61, no. 4, pp. 829–845, 2010.

[16] P. Gardonio, S. J. Elliott, and R. J. Pinnington, "Active isolation of structural vibration on a multiple-degree-of-freedom system .1. The dynamics of the system," *Journal of Sound and Vibration*, vol. 207, pp. 61–93, 1997.

[17] M. Kumar and A. S. Whittaker, "Cross-platform implementation, verification and validation of advanced mathematical models of elastomeric seismic isolation bearings," *Engineering Structures*, vol. 175, pp. 926–943, 2018.

[18] E. N. Farsangi, A. A. Tasnimi, T. Y. Yang, I. Takewaki, and M. Mohammadhasani, "Seismic performance of a resilient low-damage base isolation system under combined vertical and horizontal excitations," *Smart Structures and Systems*, vol. 22, pp. 383–397, 2018.

[19] JN. Yang and A. K. Agrawal, "Protective systems for high-technology facilities against microvibration and earthquake," *Structural Engineering & Mechanics*, vol. 10, no. 6, pp. 561–575, 2000.

[20] J. Yao, L. Fang, and R. Zhang, "Building vibration prediction induced by moving train with random forest," *Journal of Advanced Transportation*, vol. 2021, pp. 1–13, 2021.

[21] S. Deshpande, S. Mehta, and G. N. Jazar, "Optimization of secondary suspension of piecewise linear vibration isolation systems," *International Journal of Mechanical Sciences*, vol. 48, no. 4, pp. 341–377, 2006.

[22] J. Forrest and H. Hunt, "Ground vibration generated by trains in underground tunnels," *Journal of Sound and Vibration*, vol. 294, no. 4-5, pp. 706–736, 2006.

[23] N. Zhang, h. Xia, W. G. Yang, and S. Zhao, "Prediction and control of building vibration under metro excitations," in *Proceedings of the 8 Th International Conference on Structural Dynamics (EURODYN 2011)*, pp. 705–711, Leuven, Belgium, July 2011.